



Graphene quantum dots as autophagy-inducing photodynamic agents

Zoran M. Markovic^{a,*}, Biljana Z. Ristic^{b,1}, Katarina M. Arsikin^{b,1}, Djordje G. Klisic^c, Ljubica M. Harhaji-Trajkovic^d, Biljana M. Todorovic-Markovic^a, Dejan P. Kepic^a, Tamara K. Kravic-Stevovic^e, Svetlana P. Jovanovic^a, Marina M. Milenkovic^b, Dusan D. Milivojevic^a, Vladimir Z. Bumbasirevic^e, Miroslav D. Dramicanin^a, Vladimir S. Trajkovic^{b,**}

^a Vinca Institute of Nuclear Sciences, University of Belgrade, 11000 Belgrade, Serbia

^b Institute of Microbiology and Immunology, School of Medicine, University of Belgrade, 11000 Belgrade, Serbia

^c School of Electrical Engineering, University of Belgrade, 11000 Belgrade, Serbia

^d Institute for Biological Research, University of Belgrade, 11000 Belgrade, Serbia

^e Institute of Histology and Embryology, School of Medicine, University of Belgrade, 11000 Belgrade, Serbia

ARTICLE INFO

Article history:

Received 1 June 2012

Accepted 22 June 2012

Available online 15 July 2012

Keywords:

Carbon
Nanoparticle
Photosensitisation
Cytotoxicity
Apoptosis

ABSTRACT

The excellent photoluminescent properties of graphene quantum dots (GQD) makes them suitable candidates for biomedical applications, but their cytotoxicity has not been extensively studied. Here we show that electrochemically produced GQD irradiated with blue light (470 nm, 1 W) generate reactive oxygen species, including singlet oxygen, and kill U251 human glioma cells by causing oxidative stress. The cell death induced by photoexcited GQD displayed morphological and/or biochemical characteristics of both apoptosis (phosphatidylserine externalization, caspase activation, DNA fragmentation) and autophagy (formation of autophagic vesicles, LC3-I/LC3-II conversion, degradation of autophagic target p62). Moreover, a genetic inactivation of autophagy-essential LC3B protein partly abrogated the photodynamic cytotoxicity of GQD. These data indicate potential usefulness of GQD in photodynamic therapy, but also raise concerns about their possible toxicity.

© 2012 Elsevier Ltd. All rights reserved.

1. Introduction

Because of their optical properties, semiconductor quantum dots (e.g. CdSe) have recently gained considerable attention in the field of nanomedicine as bioimaging probes [1]. However, the biomedical applicability of CdSe quantum dots has been greatly limited by the release of cadmium and ensuing toxicity [2,3]. Recently, a class of carbon nanoparticles superior to conventional semiconductor quantum dots in terms of chemical inertness and biocompatibility, have been synthesized and named carbon dots [4–6]. Their favorable characteristics also include size- and wavelength-dependent luminescence, resistance to photo-bleaching and ease of production and bioconjugation. In addition, a carbon dot subclass called graphene quantum dots (GQD) have the special physico-chemical properties of graphene, a single layer

of carbon atoms in a honeycomb structure, with large surface area and excellent thermal/chemical stability [7]. For these reasons, carbon dots/GQD synthesized by various top-down and bottom-up approaches [4–6] are presently at the center of significant research efforts to develop low-toxicity, environmentally friendly alternatives of conventional semiconductor quantum dots.

Interestingly, in addition to their excellent photoluminescent properties, GQD have been recently found to act both as electron donors and electron acceptors [8], indicating their prooxidant and antioxidant potential. Accordingly, Christensen et al. have demonstrated that laser ablation-produced GQD with the surface passivated by polyethylene glycol were able to both quench and produce reactive oxygen species (ROS) in cell-free conditions, the latter occurring upon irradiation with blue light [9]. These data suggest that GQD might be potential candidates for photodynamic therapy, in which the light energy is converted by a photosensitizer to production of ROS, such as singlet oxygen (¹O₂), which kills nearby cells [10]. Photodynamic therapy is recognised as a minimally invasive and minimally toxic therapeutic strategy for the selective destruction of cancerous and various nonneoplastic lesions [10,11]. However, while conventional quantum dots, as well as C₆₀ fullerenes, the spherical cage-like carbon molecules, have

* Corresponding author. Tel.: +381 11 2455 451; fax: +381 11 3440 100.

** Corresponding author. Tel.: +381 11 3643 233; fax: +381 11 3643 235.

E-mail addresses: zormark@vinca.rs (Z.M. Markovic), vtrajkovic@eunet.rs (V.S. Trajkovic).

¹ These authors equally contributed to the work.

both been proposed as candidate photosensitizer drugs [12–14], the photodynamic cytotoxicity of GQD has not been demonstrated so far.

In the present study, we used an *in vitro* system to investigate the ability of GQD to cause death of mammalian cells upon photoirradiation, as well as to analyze the molecular mechanisms of GQD-mediated photodynamic cytotoxicity.

2. Materials and methods

2.1. Preparation and characterization of GQD

A stable ethanol suspension of GQD was prepared as previously described [15], using graphite rods as both anode and cathode, and NaOH/ethanol as electrolyte, with the current intensity set to 50 mA. Equal amount of MilliQ water was added to ethanol suspension while being constantly stirred, and the more volatile ethanol was subsequently removed from the solution using rotary evaporator (the procedure was repeated 5 times). The pH value of GQD suspension was adjusted to 7.0 by addition of HCl. The total carbon particle and NaCl concentration in the obtained suspension was adjusted to 1 mg/ml and 0.9%, respectively. Control solution was prepared in an identical way starting from 0.9% NaOH solution in ethanol, but excluding the step of electrophoresis of graphite electrode. A single GQD monolayer thin film deposited on mica (air-dried at 2000 °C for 10 min) was analyzed by atomic force microscopy (AFM) using a Quesant AFM (Agoura Hills, CA) operating in tapping mode in air at room temperature, with standard silicon tips (NanoAndMore GmbH, Wetzlar, Germany) with the force constant of 40 N/m. The images of GQD on the formvar-coated grids were obtained using a Morgagni 268(D) transmission electron microscope (FEI, Hillsboro, OR). The UV–Vis spectra of the GQD suspensions were scanned within the wavelength range of 260–510 nm at 20 °C and automatically corrected for the suspending medium, using Avantes UV–Vis spectrophotometer (Apeldoorn, The Netherlands). The luminescence emission measurements were performed at room temperature on the Fluorolog-3 FL3-221 spectrofluorometer system (Horiba Jobin-Yvon S.A.S., Chilly Mazarin, France), utilizing a 450 W Xenon lamp as excitation source (328 nm) and R928P photomultiplier tube as a detector. The electron paramagnetic resonance (EPR) analysis was performed on dry GQD samples in solid state, using a Magnetech spectrometer (Magnetech GmbH, Berlin, Germany). EPR was also employed for detection of singlet oxygen production by GQD, using 2,2,6,6-tetramethylpiperidine (TMP) as a spin trap to scavenge $^1\text{O}_2$, causing a formation of the stable nitroxide radical TEMPOL and the consequent hyperfine splitting of the EPR signal into three narrow lines [16]. A mixture containing 0.18 ml TMP (Sigma–Aldrich, St. Louis, MO) and 2 ml of GQD suspension (1 mg/ml) was ultrasonicated and illuminated using the in-house-built blue lamp with 1 W blue LED (465–475 nm) at room temperature for 30 min. Aliquots (7 μl) of the TMP-GQD mixtures were then transferred into 3 mm i.d. quartz tubes and the TEMPOL signal was analyzed on a Magnetech spectrometer, using as a control the mixture of TMP and control solution without GQD.

2.2. Cells and cell cultures

The human glioblastoma cell line U251 was kindly donated by Dr. Pedro Tranque (Universidad de Castilla-La Mancha, Albacete, Spain). Cells were maintained at 37 °C in a humidified atmosphere with 5% CO_2 , in a HEPES-buffered RPMI 1640 cell culture medium with L-glutamine supplemented with 5% fetal calf serum (FCS), 1 mM sodium pyruvate and penicillin/streptomycin (all from Sigma–Aldrich, St. Louis, MO). The cells were detached by conventional trypsinization procedure, resuspended in phosphate buffered saline (PBS) with 5% FCS and transferred in 200 μl aliquots (4×10^5 cells) to 15 ml glass centrifuge tubes. Then, 200 μl of PBS (5% FCS) without (control) or with GQD were added and the obtained suspensions exposed to blue light (465–475 nm, 1 W). After irradiation, cell suspensions were diluted in cell culture medium and transferred to 96-well plates (2×10^4 cells/well in 200 μl) for cell viability assays, 24-well plates (1×10^5 cells/well in 1 ml) for the flow cytometry, or 90 mm cell culture dishes (2×10^6 cells in 10 ml) for the immunoblotting. L-ascorbic acid (Sigma–Aldrich) was used in some experiments. The incubation times and concentrations of agents are stated in figure legends and/or figures.

2.3. Determination of cell viability

The crystal violet, MTT [3-(4,5-dimethylthiazol-2-yl)-2,5-diphenyltetrazolium bromide], acid phosphatase and lactate dehydrogenase (LDH) release assays were used to assess cell number, mitochondrial dehydrogenase activity, intracellular acid phosphatase activity and cell membrane integrity, respectively, as markers of cell viability. The tests were performed exactly as previously described [17,18] and the results were presented as % of the control viability (crystal violet, MTT) arbitrarily set to 100%, or as % cytotoxicity (LDH), using Tryton X-100-lysed untreated cells as a positive control.

2.4. Flow cytometric analysis of apoptosis

Flow cytometric analysis was performed on a FACSCalibur flow cytometer (BD Biosciences, Heidelberg, Germany), using a CellQuest Pro software for acquisition and analysis. The size and granularity of cells were assessed using forward scatter (FSC) and side scatter (SSC) analysis, respectively. Apoptotic cell death was analyzed by double staining with Annexin V-fluorescein isothiocyanate (FITC) and propidium iodide, in which the former binds to early apoptotic cells with exposed phosphatidylserine, while the latter labels the late apoptotic/necrotic cells with membrane damage. Staining was performed according to the instructions by the manufacturer (BD Pharmingen, San Diego, CA). Activation of caspases was measured by flow cytometry after labeling the cells with a cell-permeable, FITC-conjugated pan-caspase inhibitor (ApoStat; R&D Systems, Minneapolis, MN) according to the manufacturer's instructions.

2.5. Reactive oxygen species (ROS) determination

Intracellular production of ROS was determined by measuring the intensity of green fluorescence emitted by the redox-sensitive dyes dihydrodihydroamine 123 (DHR) and 2',7'-dichlorofluorescein diacetate (DCFDA), while superoxide generation was measured using dihydroethidium (DHE) (all from Invitrogen, Paisley, UK) exactly as previously described [19,20]. The mean intensity of green (FL1-DHR and DCFDA) or red (FL2-DHE) fluorescence, corresponding to total ROS or superoxide levels, respectively, was determined using a FACSCalibur flow cytometer. Alternatively, DHR was used to determine ROS in the cell-free conditions, using Chameleon (Hidex, Turku, Finland) fluorescence reader (488 nm excitation, 530 nm detection).

2.6. Transmission electron microscopy (TEM) and confocal microscopy

For the TEM analysis, trypsinized cells were fixed with 3% glutaraldehyde in phosphate-buffered saline and postfixed in 1% OsO_4 . After dehydration in graded alcohols, thin sections were embedded in Epon 812 (Agar Scientific, Stansted, UK) and stained with uranyl acetate/lead citrate for TEM analysis. For confocal microscopy, cells were cultured in chamber plates, fixed in 4% paraformaldehyde, and examined using a Leica TCS SP2 laser confocal microscope (Leica, Wetzlar, Germany).

2.7. Immunoblot analysis

Immunoblot detection of microtubule-associated protein 1 light-chain 3B (LC3B), p62 and β -actin in cell lysates was performed as previously described [21], using appropriate primary antibodies and peroxidase-conjugated goat anti-rabbit IgG as the secondary antibody (all from Cell Signaling Technology, Cambridge, MA). The specific protein bands were visualized using the Amersham reagent for enhanced chemiluminescence (GE Healthcare, Little Chalfont, UK).

2.8. RNA interference

U251 cells stably expressing lentiviral vector plasmids encoding LC3B short hairpin RNA (shRNA) or control plasmids (both from Santa Cruz Biotechnology, Santa Cruz, CA) were generated according to the manufacturer's instructions.

2.9. Statistical analysis

The statistical significance of the differences between treatments was assessed using one-way ANOVA followed by Student–Neuman–Keuls test for multiple comparisons. The value of $p < 0.05$ was considered significant.

3. Results and discussion

3.1. Synthesis and characterization of GQD

The GQD particles produced by electrochemical oxidation of graphite were oval-shaped with the average particle diameter of 56.6 ± 8.7 nm and the average height of 1.9 ± 0.8 nm (mean \pm SD, $n = 100$), as demonstrated by AFM analysis (Fig. 1A). Similar results (particle diameter ~ 60 nm) were obtained with TEM (Fig. 1B). UV–Vis analysis demonstrated that the absorbance was highest in the UV part of the spectrum, exponentially decreasing while approaching the higher wavelengths (Fig. 1C), thus conforming to previous reports [22]. In accordance with the previous measurements performed in similar conditions [15], the photoluminescence spectrums have shown that GQD have highest luminescence in the visible part of the spectrum, with the maximum at 460 nm (Fig. 1D). The observed blue photoluminescence may originate from the free zigzag sites with a carbene-like triplet ground state. The EPR

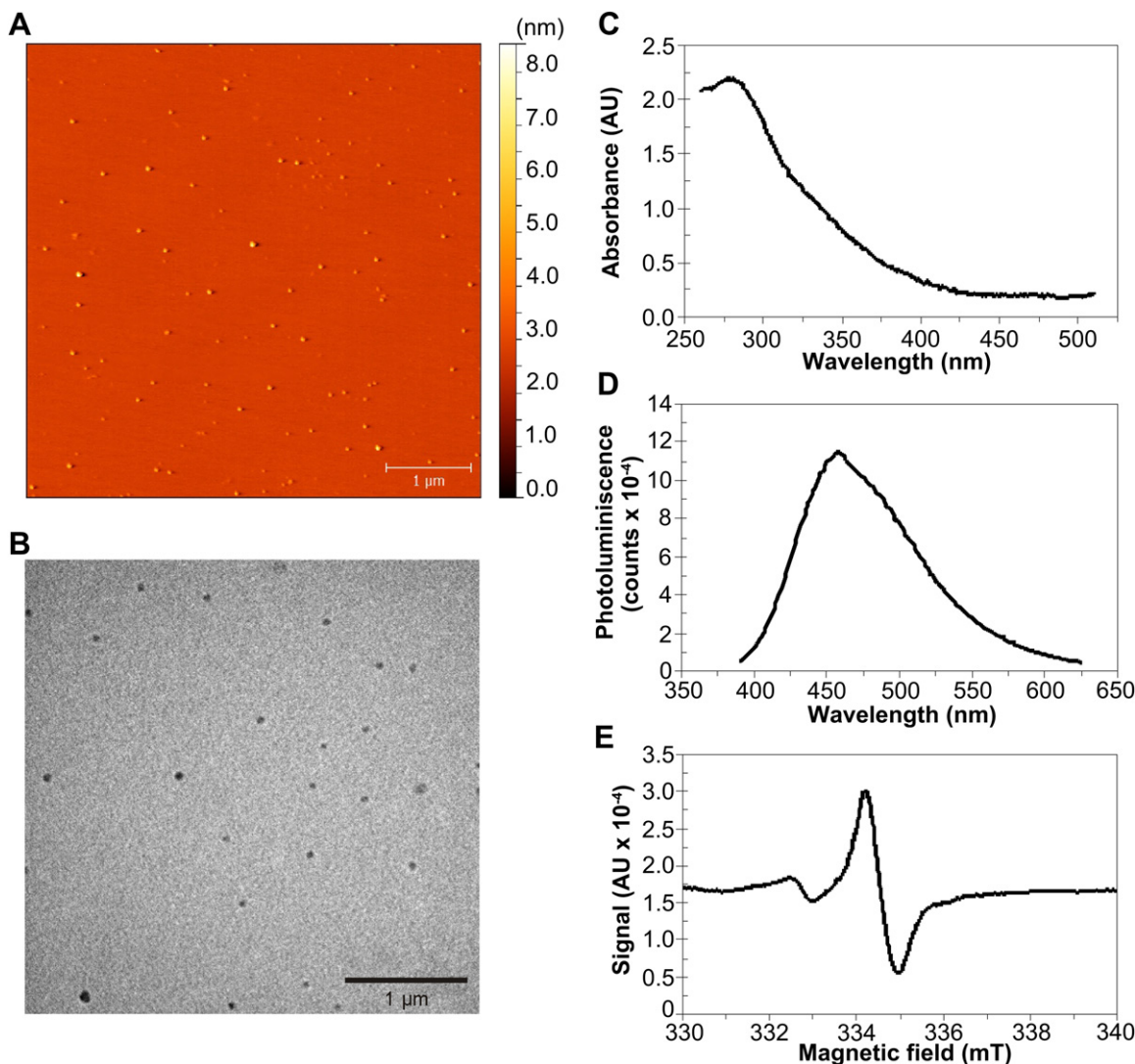


Fig. 1. Characterization of GQD. AFM (A), TEM (B), UV–Vis (C), photoluminescence (D) and EPR (E) analysis of electrochemically prepared GQD (AU, arbitrary units).

analysis revealed a narrow derivative signal of Lorentzian shape centered at $g = 2.0051$ (Fig. 1E), which is consistent with the presence of carbon free radicals at the GQD surface.

3.2. ROS production by photoexcited GQD

The presence of the defects and free radicals at the surface of GQD indicates their potential for singlet oxygen generation. Accordingly, Christensen et al., using fluorescent dyes singlet oxygen sensor green and DHR, have recently demonstrated that laser ablation-produced GQD with the surface passivated by polyethylene glycol can produce $^1\text{O}_2$ upon excitation with blue light [9]. We sought to confirm if this also applies to electrochemically-generated GQD by using DHR, a redox-sensitive dye that emits green fluorescence when oxidized by various ROS, including singlet oxygen [23]. Our results demonstrate a significant concentration-dependent increase in DHR fluorescence of laser light (488 nm)-excited GQD compared to control samples without GQD or DHR (Fig. 2A), indicating generation of ROS. However, as some ROS-detecting fluorescent dyes have been found to yield false positive results when used with carbon nanomaterials [24], we additionally employed a spin trap-based EPR spectroscopy as a sensitive and

selective method for $^1\text{O}_2$ detection. The amplitude of the EPR signal produced by blue light (470 nm)-irradiated GQD was higher than that of the control sample (Fig. 2B), thus demonstrating the ability of GQD to generate singlet oxygen upon photoexcitation. Therefore, electrochemically-generated GQD produce ROS when photo-stimulated, and at least part of the observed ROS production could be ascribed to singlet oxygen.

3.3. Induction of oxidative stress-mediated apoptosis by photoexcited GQD

The ability of GQD to generate singlet oxygen upon photoexcitation prompted us to investigate their photodynamic cytotoxicity, using U251 human glioma cells as a model system. Treatment with GQD or blue light alone did not significantly affect the viability of U251 cells, as determined by the panel of cytotoxicity/viability assays (Fig. 3A–E). On the other hand, simultaneous treatment with GQD and blue light markedly reduced cellular viability, depending both on the duration of photoexposure (Fig. 3A–D) and the concentration of GQD (Fig. 3E). The analysis of cell morphology by optical microscopy confirmed these findings, showing that the cells exposed to photoexcited GQD lost their normal polygonal shape

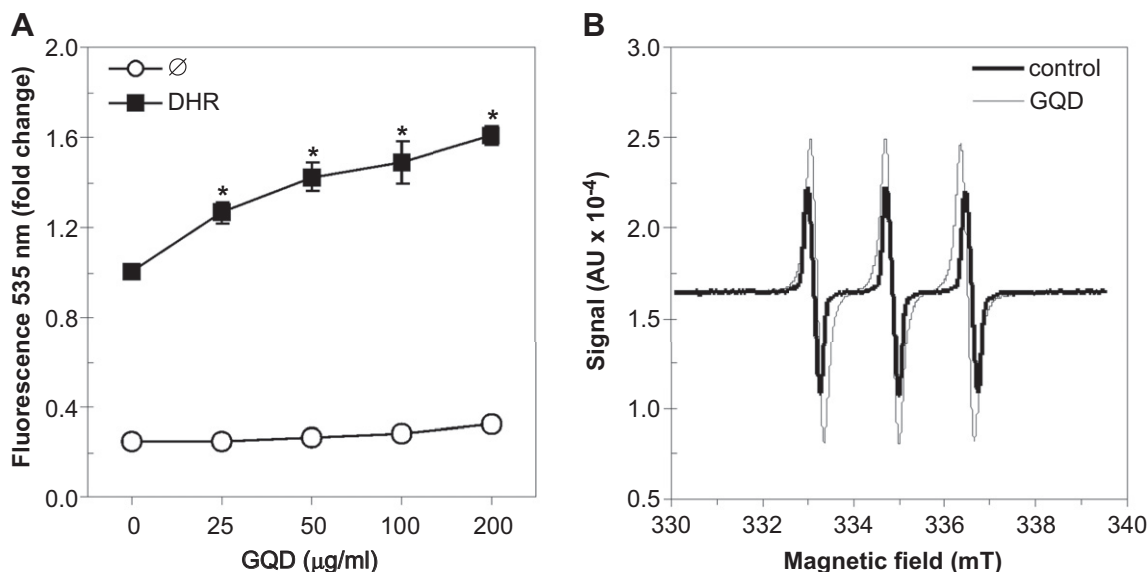


Fig. 2. ROS production by photoexcited GQD in cell-free conditions. (A) GQD suspension was mixed with a redox-sensitive fluorochrome DHR (2 µM) or equivalent amount of vehicle (dimethyl sulfoxide) and the intensity of green fluorescence (535 nm) was measured in a fluorescence reader equipped with 488 nm excitation laser. Data are mean ± SD values of triplicates from a representative of three independent experiments (* $p < 0.05$). (B) EPR analysis of singlet oxygen production in light-irradiated (470 nm, 1 W, 30 min) GQD and control solution (AU, arbitrary units).

and became round and smaller (Fig. 3F). No significant increase in temperature was observed in cell suspension exposed to photoexcited GQD (data not shown), thus ruling out the possibility of photothermal toxicity. To assess if GQD photodynamic cytotoxicity was due to induction of programmed cell death type I, known as apoptosis, we employed a flow cytometric analysis of cell size/granularity, Annexin V-detectable phosphatidylserine presence on the outer cell membrane, DNA fragmentation in propidium iodide-stained cells, and caspase activation in cells stained with the fluorescent caspase inhibitor [25]. In agreement with the preserved viability of cells incubated with non-irradiated GQD (Fig. 3), GQD did not cause significant changes in apoptotic parameters in the absence of photoexcitation (data not shown). Therefore, in order to compensate for the intrinsic GQD fluorescence, all flow cytometry analyses were done comparing the non-irradiated and photo-irradiated cell suspensions containing GQD. The cell size (FSC) was reduced, while cell granularity (SSC) was increased upon exposure to photoirradiated GQD (Fig. 4A), which is characteristic for the apoptotic cell death [26]. Accordingly, the treatment with photoexcited GQD was associated with the increase in numbers of both early (propidium iodide⁻) and late (propidium iodide⁺) apoptotic cells expressing phosphatidylserine (Annexin⁺) (Fig. 4B), as well as with the increase in DNA fragmentation (sub-G compartment of the cell cycle) (Fig. 4C) and the activation of apoptosis-executing enzymes of the caspase family (Fig. 4D). The increase in intracellular fluorescence of redox-sensitive dyes DHR and DCFDA confirmed that phototoxicity of GQD was associated with ROS generation (Fig. 5A, B). The fluorescence of superoxide-sensitive DHE [27] was also increased in cells exposed to photoexcited GQD (Fig. 5C), thus indicating that at least part of the ROS production could be ascribed to generation of superoxide anion radical ($\cdot\text{O}_2^-$). L-ascorbic acid, a well-known antioxidant [28], significantly protected U251 cells from photoirradiated GQD (Fig. 5D, E), suggesting the involvement of oxidative stress in their photodynamic cytotoxicity. While these findings are generally consistent with the results obtained in cell-free conditions (Fig. 2), it should be noted that the ability of GQD to induce oxidative stress appeared disproportionately high in comparison with its capacity for

singlet oxygen generation measured by EPR. This could be due to the possibility that some other ROS different from $^1\text{O}_2$ was actually responsible for the cytotoxicity of photoexcited GQD. For example, the triplet excited state of C_{60} , generated from the singlet excited state initially formed upon light excitation, is an excellent electron acceptor, yielding a reduced fullerene triplet ($^3\text{C}_{60}^-$) that can readily transfer an electron to molecular oxygen to form superoxide anion radical [29]. This type of reaction, in contrast to singlet oxygen generation, preferentially occurs in polar solvents, particularly in the presence of reducing agents such as NADH [30,31]. Although the exact mechanisms of photoinduced ROS generation by GQD have not been explored thus far, it is conceivable to assume that they might be similar to those described for fullerenes. This assumption is supported by the fact that GQD could actually be produced directly from fullerenes [32]. It is therefore possible that superoxide, rather than singlet oxygen, was the main reactive oxygen mediator responsible for the proapoptotic activity of photoexcited GQD. Also, there is a positive feedback for the enhanced superoxide production by oxidatively damaged mitochondria [33], which can further contribute to oxidative stress triggered by GQD.

3.4. The role of autophagy in the intracellular localization and phototoxicity of GQD

It has previously been reported that surface-passivated carbon dots can gain access to intracellular space, but their specific localization has not been investigated [34]. Therefore, to get an additional insight into the mechanisms of GQD photodynamic cytotoxicity, we investigated their intracellular localization. After incubation of U251 cells with photoexcited GQD for 4 h, examination under confocal microscope revealed a significant accumulation of cell-associated GQD displaying green fluorescence (Fig. 6A). This was confirmed by flow cytometry analysis, which demonstrated a clear increase in green fluorescence in U251 cells incubated with GQD (Fig. 6B). We next used TEM to determine intracellular localization of GQD more precisely. In comparison with control cells (Fig. 6C), the cells incubated with photoexcited GQD displayed

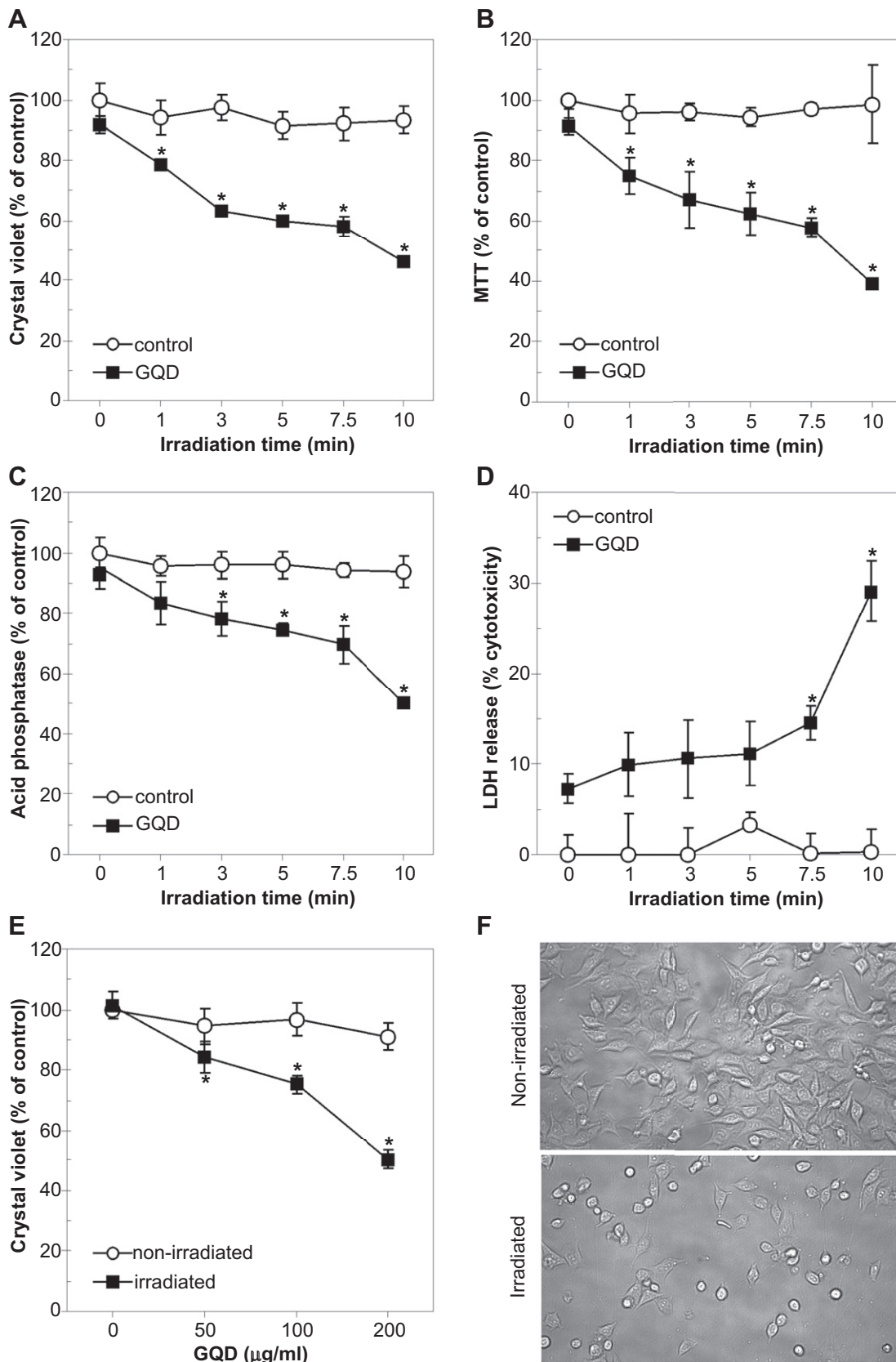


Fig. 3. Photodynamic cytotoxicity of GQD. (A–D) U251 cells were incubated with control solution or GQD (200 $\mu\text{g/ml}$) and exposed to blue light (470 nm, 1 W) for the indicated times. After 24 h, cell viability was determined by crystal violet (A), MTT (B), acid phosphatase (C) or LDH release test (D). Data are mean \pm SD values of triplicates from a representative of three independent experiments (* $p < 0.05$ refers to corresponding controls). (E, F) U251 cells were incubated with different concentrations (E) or 200 $\mu\text{g/ml}$ (F) of GQD and irradiated or not with blue light (470 nm, 1 W) for 10 min. After 24 h, cell viability was determined by crystal violet staining (E), while cell morphology was assessed by optical microscopy (F). The data in (E) are mean \pm SD values of triplicates from a representative of three independent experiments ($p < 0.05^*$ refers to corresponding non-irradiated controls).

a noticeable vacuolization after 12 h (Fig. 6D). QGD were mostly contained within numerous intracytoplasmic vesicles, indicating that internalization might have occurred via endocytosis (Fig. 6E). However, a large number of vesicles also engulfed cellular

components, such as mitochondria (Fig. 6E, F), thus resembling autophagic vacuoles formed during a cellular self-digestion process called macroautophagy (autophagy) [35]. Autophagy is induced by photodynamic therapy to increase clearance of oxidatively

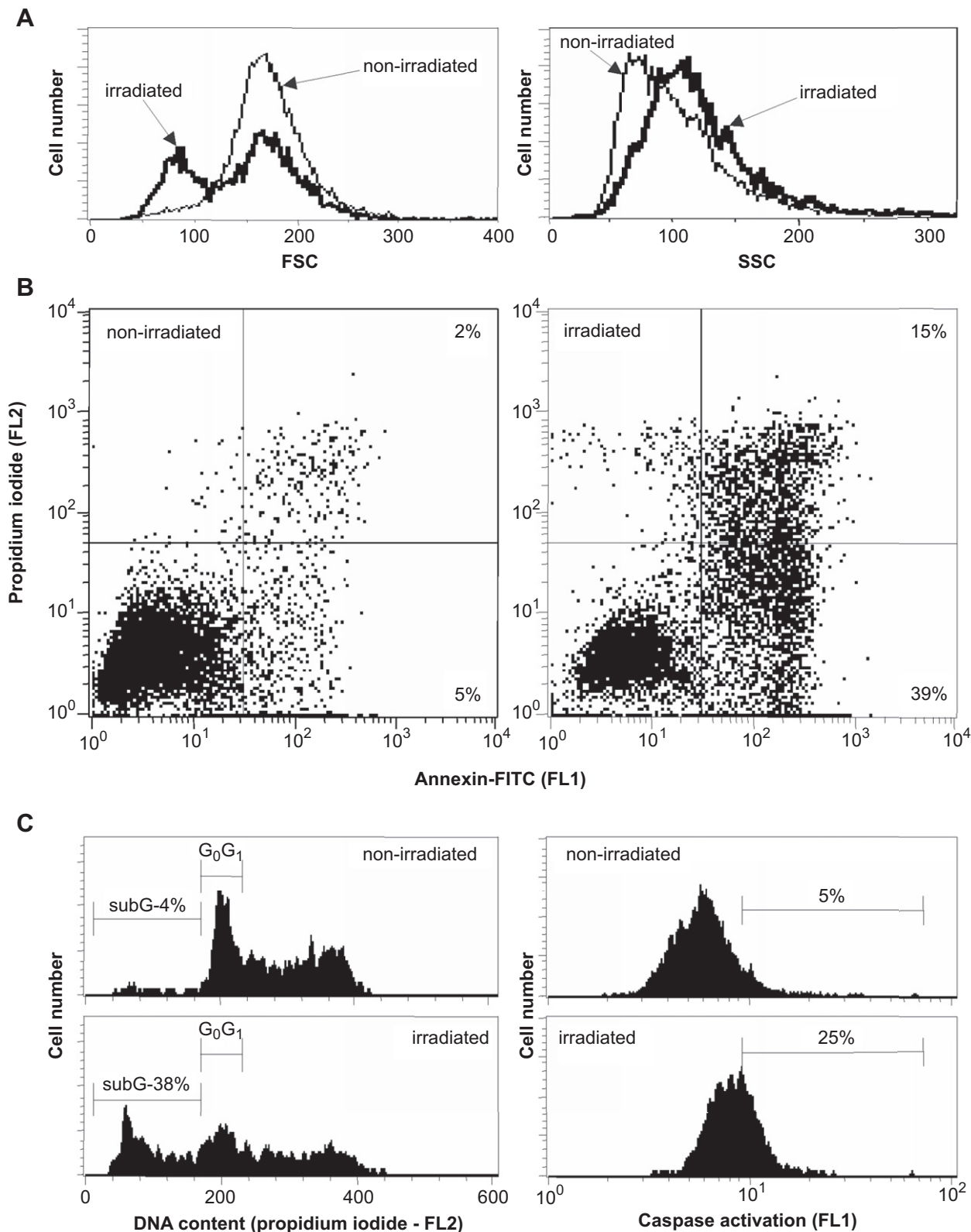


Fig. 4. Induction of apoptosis by photoexcited QGD. (A–D) U251 cells were incubated with QGD (200 µg/ml) and irradiated or not with blue light (470 nm, 1 W) for 10 min. After 24 h, cell size (FSC) and granularity (SSC) (A), phosphatidylserine externalization (Annexin⁺ cells) (B), DNA fragmentation (sub-G compartment) (C) and caspase activation (D) were examined by flow cytometry. The histograms and dot plots from a representative of three experiments are presented.

damaged organelles and cross-linked proteins [36], but also represents a common cellular response to nanomaterials, including classical quantum dots [37,38]. Moreover, autophagy can promote apoptotic and non-apoptotic cell death in certain conditions [39–41], and is involved in cytotoxic effects of both photodynamic and nanoparticle treatment [36,42–44]. To confirm the induction of autophagy by photoexcited GQD, we analyzed by immunoblotting the conversion of LC3B (LC3B)-I to lipidated, autophagosome-associated LC3B-II [35]. A clear time-dependent increase in the amount of LC3B-II was observed in cells exposed to photoexcited GQD in comparison to untreated cells (Fig. 6G), thus indicating an induction of the autophagic response. Furthermore, the level of

p62, the protein selectively degraded by autophagy [45], was markedly downregulated by GQD (Fig. 6G), confirming an increase in autophagic proteolysis. In order to get an insight into the role of autophagy in photodynamic cytotoxicity of GQD, we used RNA interference to block the expression of the autophagy-essential LC3B. U251 cells stably transfected with short hairpin RNA against LC3B expressed less LC3B and were significantly protected from the photodynamic cytotoxicity of GQD, as demonstrated by crystal violet staining (Fig. 6H). These results clearly show that photoexcited GQD can readily gain access to target cells, initiating an autophagic response that contributes to the observed photodynamic cytotoxicity. Finally, it should be noted that the results

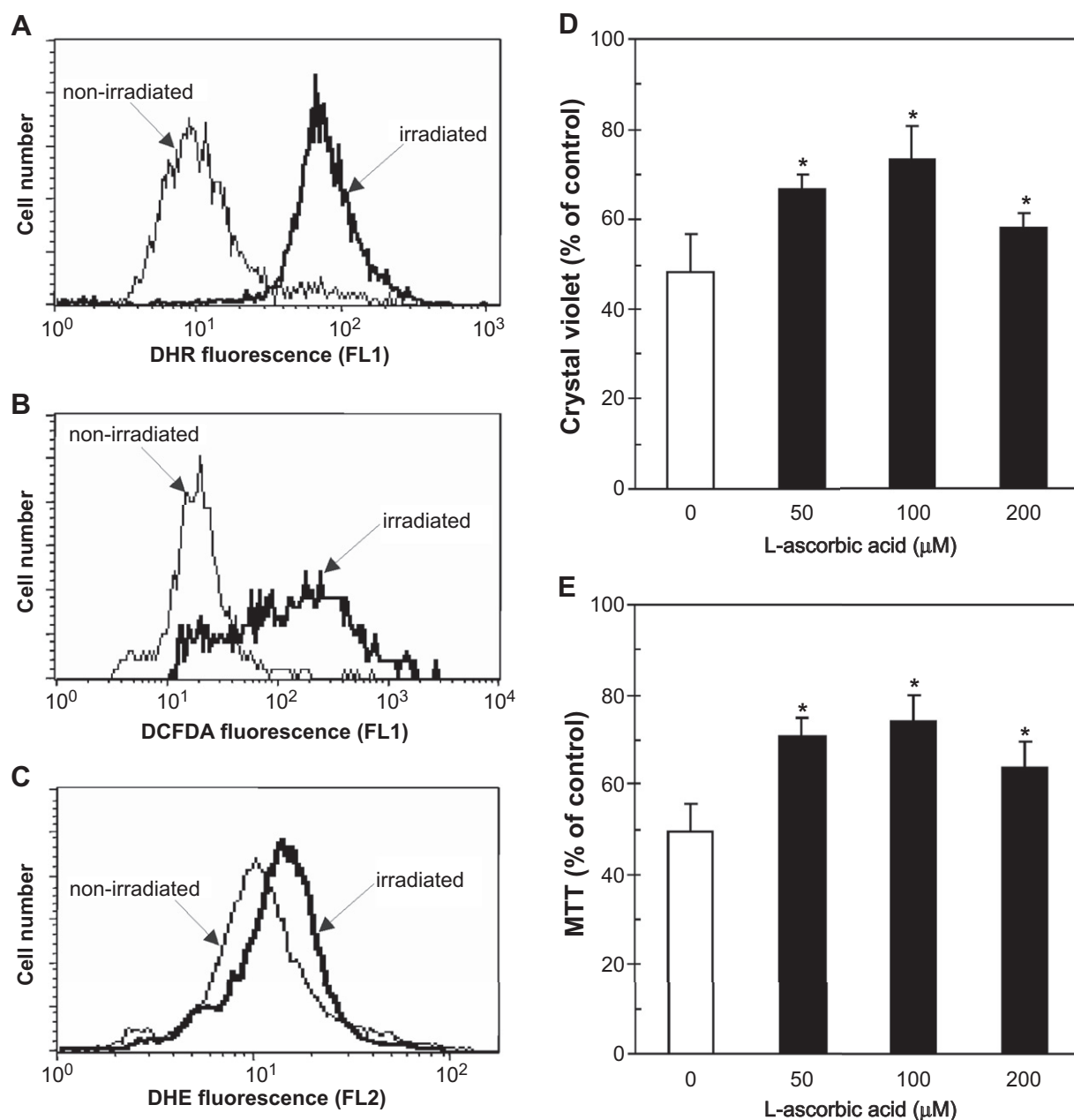


Fig. 5. Involvement of oxidative stress in phototoxicity of GQD. (A–C) U251 cells were incubated with GQD (200 $\mu\text{g}/\text{ml}$) and irradiated or not with blue light (470 nm, 1 W) for 10 min. Intracellular production of ROS (A, B) and superoxide (C) was determined after 4 h by flow cytometry and the histograms from a representative of three experiments are presented. (D, E) U251 cells were pre-incubated or not with the antioxidant L-ascorbic acid (50–200 $\mu\text{g}/\text{ml}$) for 6 h. Cells were then washed and GQD (200 $\mu\text{g}/\text{ml}$) were added. The suspensions were irradiated with blue light (470 nm, 1 W) for 10 min and the cell viability was assessed after 24 h by crystal violet staining and MTT test. Data are mean \pm SD values of triplicates from a representative of three independent experiments (* $p < 0.05$).

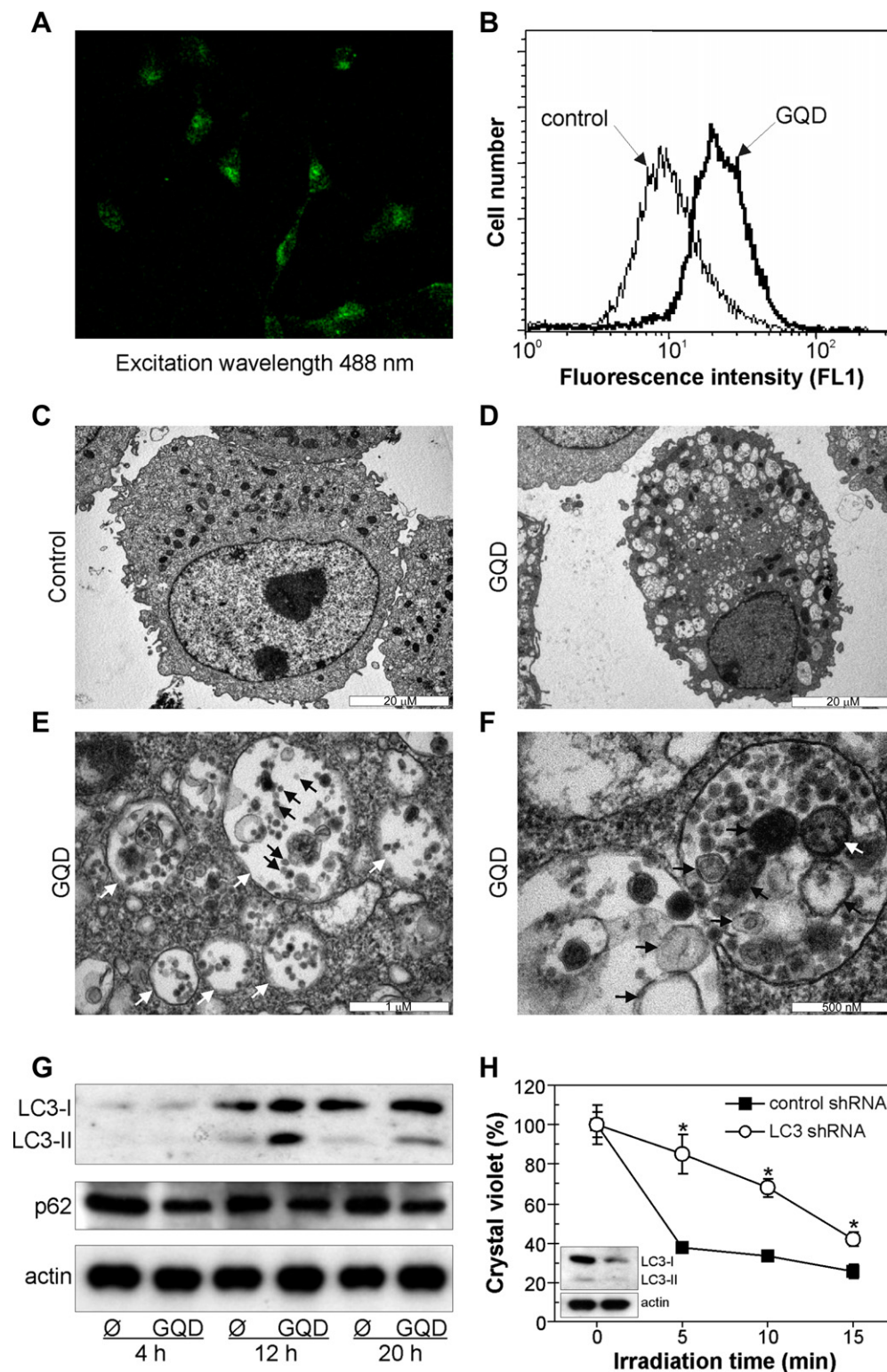


Fig. 6. The role of autophagy in the intracellular localization and phototoxicity of GQD. (A, B) U251 cells were incubated with GQD (200 µg/ml) or control solution and irradiated with blue light (470 nm, 1 W) for 10 min. After 4 h, the intensity of GQD-emitted green fluorescence (530 nm) was monitored by confocal microscopy (A) or flow cytometry (B). (C–F) U251 cells were incubated with control solution (C) or 200 µg/ml GQD (D–F) and irradiated with blue light (470 nm, 1 W) for 10 min. After 12 h, the intracellular localization of GQD was assessed by TEM. White arrows in (E) point to intracellular vesicles engulfing GQD (black arrows). (F) Autophagic vacuoles containing both GQD and cellular components (black arrows), including mitochondria (white arrow). (G) Immunoblot analysis of LC3 conversion and p62 level in U251 cells incubated with control solution or GQD (200 µg/ml) and exposed to blue light (470 nm, 1 W) for 10 min. (H) U251 cells stably transfected with control or LC3B shRNA (the insert shows immunoblot confirmation of LC3B knockdown) were incubated with GQD (200 µg/ml) and exposed to blue light (470 nm, 1 W) for the indicated times. Cell viability was determined after 24 h by crystal violet staining. Data are mean \pm SD values of triplicates from a representative of three independent experiments (* p < 0.05 refers to cells transfected with control shRNA).

similar to those presented in Figs. 3–6 were also obtained in L929 mouse fibrosarcoma cell line (data not shown), indicating that the observed effects were not species- or cell type-specific.

4. Conclusions

The present study describes the *in vitro* photodynamic cytotoxicity of GQD, mediated by induction of oxidative stress and subsequent activation of both type I (apoptosis) and type II (autophagy) programmed cell death. In view of the increasing interest for biomedical applications of GQD, this feature could be exploited in photodynamic therapy, but also raises a concern about their potential toxicity.

Acknowledgments

The authors thank Nikola Davidovac (Castanea, Belgrade, Serbia) for building the lamp used for photoexcitation. This work was supported by the Ministry of Education and Science of the Republic of Serbia (grants 41025 to VT, 172003 to BTM and 173053 to LHT).

References

- Alivisatos AP, Gu W, Larabell C. Quantum dots as cellular probes. *Annu Rev Biomed Eng* 2005;7:55–76.
- Derfus AM, Chan WCW, Bhatia SN. Probing the cytotoxicity of semiconductor quantum dots. *Nano Lett* 2004;4:11–8.
- Lovric J, Cho SJ, Winnik FM, Maysinger D. Unmodified cadmium telluride quantum dots induce reactive oxygen species formation leading to multiple organelle damage and cell death. *Chem Biol* 2005;12:1227–34.
- Baker SN, Baker GA. Luminescent carbon nanodots: emergent nanolights. *Angew Chem Int Ed Engl* 2010;49:6726–44.
- Shen J, Zhu Y, Yang X, Li C. Graphene quantum dots: emergent nanolights for bioimaging, sensors, catalysis and photovoltaic devices. *Chem Commun (Camb)* 2012;48:3686–99.
- Esteves da Silva JCG, Goncalves HMR. Analytical and bioanalytical applications of carbon dots. *Trends Anal Chem* 2011;30:1327–36.
- Geim AK. Graphene: status and prospects. *Science* 2009;324:1530–4.
- Wang X, Cao L, Lu F, Mezziani MJ, Li H, Qi G, et al. Photoinduced electron transfers with carbon dots. *Chem Commun (Camb)* 2009;3774–6.
- Christensen IL, Sun YP, Juzenas P. Carbon dots as antioxidants and prooxidants. *J Biomed Nanotechnol* 2011;7:667–76.
- Agostinis P, Berg K, Cengel KA, Foster TH, Girotti AW, Gollnick SO, et al. Photodynamic therapy of cancer: an update. *CA Cancer J Clin* 2011;61:250–81.
- Verma S, Watt GM, Mai Z, Hasan T. Strategies for enhanced photodynamic therapy effects. *Photochem Photobiol* 2007;83:996–1005.
- Juzenas P, Chen W, Sun YP, Coelho MA, Generalov R, Generalova N, et al. Quantum dots and nanoparticles for photodynamic and radiation therapies of cancer. *Adv Drug Deliv Rev* 2008;60:1600–14.
- Mroz P, Tegos GP, Gali H, Wharton T, Sarna T, Hamblin MR. Photodynamic therapy with fullerenes. *Photochem Photobiol Sci* 2007;6:1139–49.
- Yaghini E, Seifalian AM, MacRobert AJ. Quantum dots and their potential biomedical applications in photosensitization for photodynamic therapy. *Nanomedicine (Lond)* 2009;4:353–63.
- Li H, He X, Kang Z, Huang H, Liu Y, Liu J, et al. Water-soluble fluorescent carbon quantum dots and photocatalyst design. *Angew Chem Int Ed Engl* 2010;49:4430–4.
- Vileno B, Jeney S, Sienkiewicz A, Marcoux PR, Miller LM, Forro L. Evidence of lipid peroxidation and protein phosphorylation in cells upon oxidative stress photo-generated by fullerenes. *Biophys Chem* 2010;152:164–9.
- Kaludjerovic GN, Miljkovic D, Momcilovic M, Djinovic VM, Mostarica Stojkovic M, Sabo TJ, et al. Novel platinum(IV) complexes induce rapid tumor cell death *in vitro*. *Int J Cancer* 2005;116:479–86.
- Yang TT, Sinai P, Kain SR. An acid phosphatase assay for quantifying the growth of adherent and nonadherent cells. *Anal Biochem* 1996;241:103–8.
- Misirlik MS, Todorovic-Markovic BM, Vucicevic LM, Janjetovic KD, Jokanovic VR, Dramicanin MD, et al. The protection of cells from nitric oxide-mediated apoptotic death by mechanochemically synthesized fullerene (C₆₀) nanoparticles. *Biomaterials* 2009;30:2319–28.
- Trpkovic A, Todorovic-Markovic B, Kleut D, Misirlik M, Janjetovic K, Vucicevic L, et al. Oxidative stress-mediated hemolytic activity of solvent exchange-prepared fullerene (C₆₀) nanoparticles. *Nanotechnology* 2010;21:375,102.
- Vucicevic L, Misirlik M, Janjetovic K, Vilimanovich U, Sudar E, Isenovic E, et al. Compound C induces protective autophagy in cancer cells through AMPK inhibition-independent blockade of Akt/mTOR pathway. *Autophagy* 2011;7:40–50.
- Li Y, Hu Y, Zhao Y, Shi G, Deng L, Hou Y, et al. An electrochemical avenue to green-luminescent graphene quantum dots as potential electron-acceptors for photovoltaics. *Adv Mater* 2011;23:776–80.
- Costa D, Fernandes E, Santos JL, Pinto DC, Silva AM, Lima JL. New noncellular fluorescence microplate screening assay for scavenging activity against singlet oxygen. *Anal Bioanal Chem* 2007;387:2071–81.
- Lyon DY, Brunet L, Hinkal GW, Wiesner MR, Alvarez PJ. Antibacterial activity of fullerene water suspensions (nC₆₀) is not due to ROS-mediated damage. *Nano Lett* 2008;8:1539–43.
- Markovic ZM, Harhaji-Trajkovic LM, Todorovic-Markovic BM, Kepic DP, Arskin KM, Jovanovic SP, et al. *In vitro* comparison of the photothermal anticancer activity of graphene nanoparticles and carbon nanotubes. *Biomaterials* 2011;32:1121–9.
- Vermes I, Haanen C, Reutelingsperger C. Flow cytometry of apoptotic cell death. *J Immunol Methods* 2000;243:167–90.
- Zhao H, Kalivendi S, Zhang H, Joseph J, Nithipatikom K, Vasquez-Vivar J, et al. Superoxide reacts with hydroethidine but forms a fluorescent product that is distinctly different from ethidium: potential implications in intracellular fluorescence detection of superoxide. *Free Radic Biol Med* 2003;34:1359–68.
- Padayatty SJ, Katz A, Wang Y, Eck P, Kwon O, Lee JH, et al. Vitamin C as an antioxidant: evaluation of its role in disease prevention. *J Am Coll Nutr* 2003;22:18–35.
- Yamakoshi Y, Sueyoshi S, Fukuhara K, Miyata N, Masumizu T, Kohno M. OH[•] and O₂^{•-} generation in aqueous C₆₀ and C₇₀ solutions by photoirradiation: an EPR study. *J Am Chem Soc* 1998;120:12,363–4.
- Yamakoshi Y, Umezawa N, Ryu A, Arakane K, Miyata N, Goda Y, et al. Active oxygen species generated from photoexcited fullerene (C₆₀) as potential medicines: O₂^{•-} versus ¹O₂. *J Am Chem Soc* 2003;125:12,803–9.
- Mroz P, Pawlak A, Satti M, Lee H, Wharton T, Gali H, et al. Functionalized fullerenes mediate photodynamic killing of cancer cells: type I versus type II photochemical mechanism. *Free Radic Biol Med* 2007;43:711–9.
- Lu J, Yeo PS, Gan CK, Wu P, Loh KP. Transforming C₆₀ molecules into graphene quantum dots. *Nat Nanotechnol* 2011;6:247–52.
- Zorov DB, Juhaszova M, Sollott SJ. Mitochondrial ROS-induced ROS release: an update and review. *Biochim Biophys Acta* 2006;1757:509–17.
- Cao L, Wang X, Mezziani MJ, Lu F, Wang H, Luo PG, et al. Carbon dots for multiphoton bioimaging. *J Am Chem Soc* 2007;129:11,318–9.
- Mizushima N, Levine B, Cuervo AM, Klionsky DJ. Autophagy fights disease through cellular self-digestion. *Nature* 2008;451:1069–75.
- Reiners Jr JJ, Agostinis P, Berg K, Oleinick NL, Kessel D. Assessing autophagy in the context of photodynamic therapy. *Autophagy* 2010;6:7–18.
- Stern ST, Zolnik BS, McLeland CB, Clogston J, Zheng J, McNeil SE. Induction of autophagy in porcine kidney cells by quantum dots: a common cellular response to nanomaterials? *Toxicol Sci* 2008;106:140–52.
- Zabirnyk O, Zeshelyev M, Seleverstov O. Nanoparticles as a novel class of autophagy activators. *Autophagy* 2007;3:278–81.
- Fimia GM, Piacentini M. Regulation of autophagy in mammals and its interplay with apoptosis. *Cell Mol Life Sci* 2010;67:1581–8.
- Ghavami S, Asoodeh A, Klonisch T, Halayko AJ, Kadkhoda K, Krocak TJ, et al. Brevinin-2R(1) semi-selectively kills cancer cells by a distinct mechanism, which involves the lysosomal–mitochondrial death pathway. *J Cell Mol Med* 2008;12:1005–22.
- Ghavami S, Eshragi M, Ande SR, Chazin WJ, Klonisch T, Halayko AJ, et al. S100A8/A9 induces autophagy and apoptosis via ROS-mediated cross-talk between mitochondria and lysosomes that involves BNIP3. *Cell Res* 2010;20:314–31.
- Khan MI, Mohammad A, Patil G, Naqvi SA, Chauhan LK, Ahmad I. Induction of ROS, mitochondrial damage and autophagy in lung epithelial cancer cells by iron oxide nanoparticles. *Biomaterials* 2012;33:1477–88.
- Liu HL, Zhang YL, Yang N, Zhang YX, Liu XQ, Li CG, et al. A functionalized single-walled carbon nanotube-induced autophagic cell death in human lung cells through Akt-TSC2-mTOR signaling. *Cell Death Dis* 2011;2:e159.
- Seleverstov O, Zabirnyk O, Zscharnack M, Bulavina L, Nowicki M, Heinrich JM, et al. Quantum dots for human mesenchymal stem cells labeling. A size-dependent autophagy activation. *Nano Lett* 2006;6:2826–32.
- Ichimura Y, Kumamidou T, Sou YS, Mizushima T, Ezaki J, Ueno T, et al. Structural basis for sorting mechanism of p62 in selective autophagy. *J Biol Chem* 2008;283:22,847–57.